JACS
JOURNAL OF THE AMERICAN CHEMICAL SOCIETY
Article
pubs.acs.org/JACS

Design and Synthesis of Bipyridine Platinum(II) Bisalkynyl Fullerene Donor–Chromophore–Acceptor Triads with Ultrafast Charge Separation

Sai-Ho Lee,[†] Chris Tsz-Leung Chan,[‡] Keith Man-Chung Wong,[†] Wai Han Lam,[†] Wai-Ming Kwok,*[,‡] and Vivian Wing-Wah Yam*[,†]

[†]Department of Chemistry, The University of Hong Kong, Pokfulam Road, Hong Kong, P.R. China

[‡]Department of Applied Biology and Chemical Technology, The Hong Kong Polytechnic University, Hung Hom, Kowloon, Hong Kong, P.R. China

Supporting Information

ABSTRACT: Donor–chromophore–acceptor triads, **(PTZ)$_2$-Pt(bpy)-C$_{60}$** and **(^{t}BuPTZ)$_2$-Pt(bpy)-C$_{60}$**, along with their model compound, **(Ph)$_2$-Pt(bpy)-C$_{60}$**, have been synthesized and characterized; their photophysical and electrochemical properties have been studied, and the origin of the absorption and emission properties has been supported by computational studies. The photoinduced electron transfer reactions have been investigated using the femtosecond and nanosecond transient absorption spectroscopy. In dichloromethane, **(Ph)$_2$-Pt(bpy)-C$_{60}$** shows ultrafast triplet–triplet energy transfer from the ^{3}MLCT/LLCT excited state within 4 ps to give the ^{3}C$_{60}$* state, while in **(PTZ)$_2$-Pt(bpy)-C$_{60}$** and **(^{t}BuPTZ)$_2$-Pt(bpy)-C$_{60}$**, charge-separated state forms within 400 fs from the ^{3}MLCT/LLCT excited state with efficiency of over 0.90, and the total efficiency with the contribution of ^{3}C$_{60}$* is estimated to be 0.99. Although the forward electron transfer reactions are very rapid, the charge-separated state recombines to the singlet ground state at a time of hundreds of nanoseconds because of the difference in spin multiplicity between the charge-separated state and the ground state.

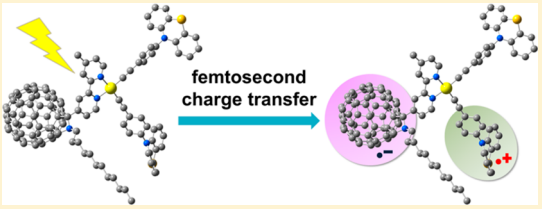

INTRODUCTION

Mimicking of the natural photosynthetic reaction center has long been an active research area.[1] The artificial models have been constructed by connecting an electron donor to an electron acceptor, which on light excitation will undergo photoinduced electron transfer reaction, many of which have proved their potential applications in photovoltaic devices.[2]

Transition metal-based chromophores, such as those of Ru(II),[3] Re(I),[4] Os(II),[5] Ir(III),[2b,3a,b,5g,6] Cu(I)[7] and Pt(II),[1c,8] have been employed in donor–acceptor systems. Because of the strong spin–orbit coupling imparted by the heavy metal centers, rapid intersystem crossing (ISC) of the singlet metal-to-ligand charge-transfer (^{1}MLCT) excited state is expected.[9] Subsequent charge transfer reactions would occur at the ^{3}MLCT excited state to form the charge-separated (CS) state in the triplet manifold. The triplet CS state should be much longer-lived than that of the corresponding singlet CS state, as the CS state and the ground state have different spin multiplicities (i.e., charge-recombination (CR) from a triplet CS state to a singlet ground state), where triplet–singlet transition is spin-forbidden. The most commonly employed metal–ligand chromophoric systems in the construction of donor–acceptor dyads or triads are those of Ru(II),[3] Re(I),[4] Os(II),[5] Ir(III),[2b,3a,b,5g,6] and Cu(I),[7] with MLCT excited states. Corresponding studies with the d^8 platinum(II) polypyridine systems, which also show MLCT excited states, are relatively less explored. Part of the reasons is associated with the poor solubility of the platinum(II) system as well as the presence of a low-lying d-d ligand-field state that quenches the ^{3}MLCT state at room temperature.[10] It was only quite recently that there has been a growing interest in the study of dyads and triads using the platinum(II) polypyridine system given the enhanced solubility and ^{3}MLCT excited state behavior of the alkynyl platinum(II) system.[9a,10e,f,11] In the current study, a bipyridine Pt(II) bisalkynyl chromophore is utilized to construct a series of donor–acceptor systems.

Recently, numerous studies have been made on transition metal-based chromophore-fullerene dyads.[2a,12] Fullerene, in particular C$_{60}$, is utilized as an electron acceptor due to its small reorganization energy for electron transfer, which results from the symmetrical shape, large size and π-electron delocalization over the three-dimensional surface.[13] In this regard, the CS state lifetime of the transition metal-based chromophore-C$_{60}$ dyads are expected to be long-lived. However, it is unfortunate that instead of the desired long-lived CS state, the localized C$_{60}$ triplet state (^{3}C$_{60}$*) has been observed in most of the dyads because of the lower-lying ^{3}C$_{60}$* (1.51 eV) energy.[2a,12]

In the present work, we extended the chromophore-C$_{60}$ dyad by the introduction of an additional electron donor to form a donor–chromophore–C$_{60}$ triad. With such modification, the energy of the final CS state would be lowered and may become

Received: April 22, 2014
Published: July 2, 2014

   dx.doi.org/10.1021/ja5040073 | J. Am. Chem. Soc. 2014, 136, 10041–10052

Chart 1

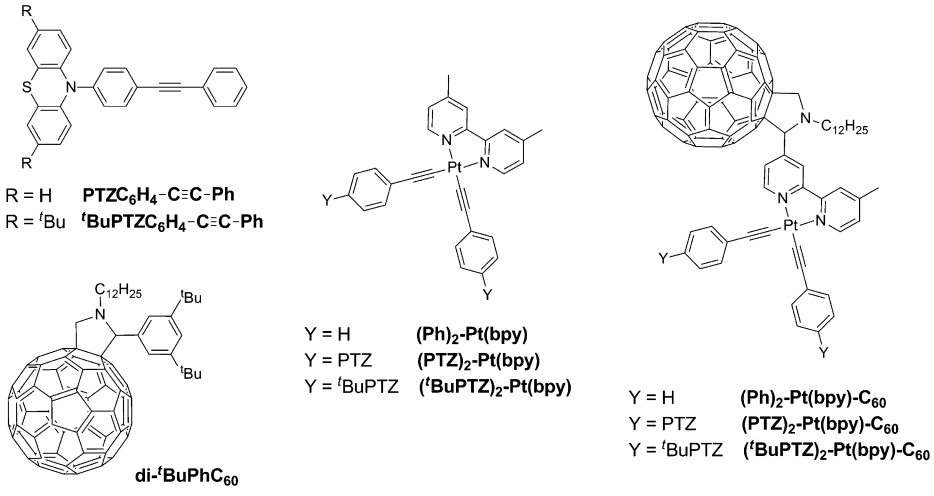

Scheme 1. Synthesis of Donor−Chromophore−Acceptor Triads, $(PTZ)_2$-Pt(bpy)-C_{60} and $(^tBuPTZ)_2$-Pt(bpy)-C_{60}[a]

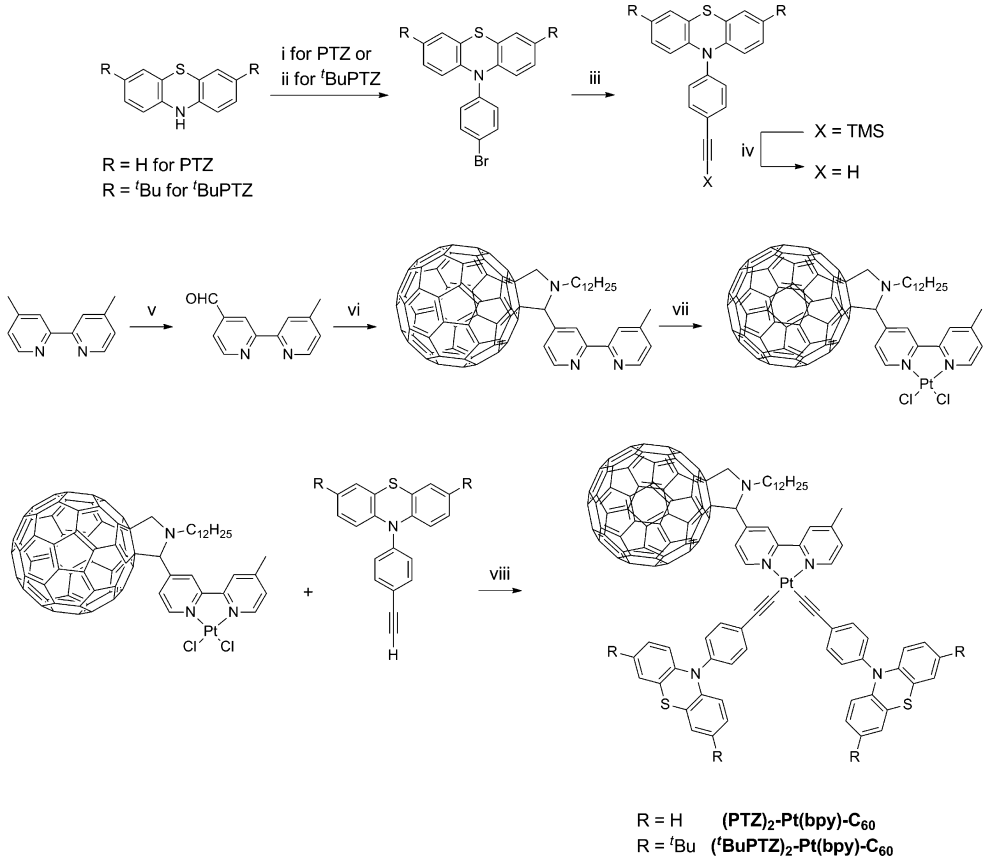

[a]Reagents and conditions: (i) 4-bromoiodobenzene, K_2CO_3, $CuSO_4{\cdot}5H_2O$, 220 °C; (ii) 4-bromoiodobenzene, K_2CO_3, 18-crown-6, Cu, DMF, reflux; (iii) $PdCl_2(PPh_3)_2$, CuI, PPh_3, TMSA, Et_3N, reflux; (iv) K_2CO_3, MeOH/THF, rt; (v) SeO_2, dioxane, reflux; (vi) *N*-dodecyl glycine, C_{60}, PhMe, reflux; (vii) $PtCl_2(DMSO)_2$, CH_2Cl_2, rt; (viii) CuI, Et_3N, CH_2Cl_2, rt.

lower than that of the $^3C_{60}$* state. Moreover, the separation of the charges may increase and may slow down the CR process. Phenothiazine (PTZ)[8b,14] along with its derivatives is a well-known heteroarene with strong electron-donating ability; therefore, in this study we developed donor−chromophore−C_{60} triads employing the PTZ moiety.

Herein, we report a detailed studies of a series of donor−chromophore−acceptor triads, **$(PTZ)_2$-Pt(bpy)-C_{60}** and **$(^tBuPTZ)_2$-Pt(bpy)-C_{60}** as well as their relevant model compounds (Chart 1) using a wide variety of experimental techniques including electronic absorption and emission spectroscopy, cyclic voltammetry, femtosecond and nanosecond time-resolved transient absorption spectroscopy, and the photochemical processes are identified and rate constants are determined. Density functional theory (DFT) and time-dependent density functional theory (TDDFT) have been

dx.doi.org/10.1021/ja5040073 | J. Am. Chem. Soc. 2014, 136, 10041−10052

performed to provide further insights into the origin of the excited states.

RESULTS AND DISCUSSION

Synthesis. The synthesis of donor−chromophore−acceptor triads, **(PTZ)$_2$-Pt(bpy)-C$_{60}$** and **(^{t}BuPTZ)$_2$-Pt(bpy)-C$_{60}$**, are outlined in Scheme 1. Various heteroarylacetylenes were first prepared utilizing Ullmann-type reaction to form the *N*-(4-bromophenyl)-heteroaryl compounds. This was followed by palladium-catalyzed Sonogashira coupling reactions with (trimethylsilyl)acetylene (TMS—C≡CH) to yield the TMS-terminated heteroarylacetylenes. The TMS group was subsequently removed by stirring with potassium carbonate in tetrahydrofuran-methanol solution. On the other hand, 4,4′-dimethyl-2,2′-bipyridine was oxidized with selenium oxide to give 4-methyl-2,2′-bipyridine-4′-carboxaldehyde, and the incorporation of fullerene was achieved by the cycloaddition of the azomethine ylide formed upon condensation of *N*-dodecyl glycine. The resulting fullerene-appended bipyridine compound was reacted with $[PtCl_2(DMSO)_2]$ to afford the dichloroplatinum(II) precursor, which was then coordinated with the alkynyls using copper-catalyzed coupling reaction.

Electronic Absorption and Emission Spectroscopy. The electronic absorption spectra of **(Ph)$_2$-Pt(bpy)**, **(PTZ)$_2$-Pt(bpy)** and **(^{t}BuPTZ)$_2$-Pt(bpy)** in dichloromethane show an intense absorption band at ca. 280−330 nm and a moderately intense band at ca. 360−450 nm with λ_{max} at ca. 400 nm (Figure 1). The high-energy intense absorption band is

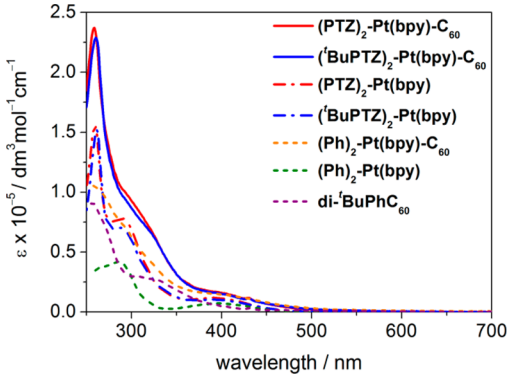

Figure 1. UV−visible absorption spectra of **(PTZ)$_2$-Pt(bpy)-C$_{60}$** and **(^{t}BuPTZ)$_2$-Pt(bpy)-C$_{60}$** as well as their model compounds of **(PTZ)$_2$-Pt(bpy)**, **(^{t}BuPTZ)$_2$-Pt(bpy)**, **(Ph)$_2$-Pt(bpy)-C$_{60}$**, **(Ph)$_2$-Pt(bpy)** and **di-^{t}BuPhC$_{60}$** in CH_2Cl_2.

assigned as the $\pi-\pi^*$ transitions of the phenothiazine, bipyridine and alkynyl moieties. On the other hand, the absorption band in the visible region is attributed to an admixture of platinum-to-bipyridine metal-to-ligand charge transfer (MLCT) and alkynyl-to-bipyridine ligand-to-ligand charge transfer (LLCT) transitions.[9a,11a,b] With the presence of the C_{60} moiety in **(Ph)$_2$-Pt(bpy)-C$_{60}$**, **(PTZ)$_2$-Pt(bpy)-C$_{60}$** and **(^{t}BuPTZ)$_2$-Pt(bpy)-C$_{60}$**, an additional absorption tail extending to 600 nm is observed, which can also be found in the electronic absorption spectrum of **di-^{t}BuPhC$_{60}$** and is tentatively assigned as the $\pi-\pi^*$ transitions of C_{60}.

To gain further insight into the nature of the electronic transitions for the complexes, computational studies were performed on selected complexes, **(Ph)$_2$-Pt(bpy)**, **(PTZ)$_2$-Pt(bpy)**, **(Ph)$_2$-Pt(bpy)-C$_{60}$** and **(PTZ)$_2$-Pt(bpy)-C$_{60}$**. For **(Ph)$_2$-Pt(bpy)-C$_{60}$** and **(PTZ)$_2$-Pt(bpy)-C$_{60}$**, the dodecyl group of *N*-dodecylpyrrolidine on C_{60} was replaced by a methyl group, and the corresponding complexes were labeled as **(Ph)$_2$-Pt(bpy)-C$_{60}$′** and **(PTZ)$_2$-Pt(bpy)-C$_{60}$′** (see Computational Details).

The highest occupied molecular orbital (HOMO) and HOMO−1 of **(Ph)$_2$-Pt(bpy)** are the π orbitals of the phenylalkynyl ligands mixed with the platinum dπ orbitals, while the HOMO and HOMO−1 of **(PTZ)$_2$-Pt(bpy)** correspond to the π orbitals mainly localized on the phenothiazine entities, owing to the excellent electron-donating ability of phenothiazine (Figures S1 and S2, Supporting Information). For **(Ph)$_2$-Pt(bpy)-C$_{60}$′** (Figure S3, Supporting Information) and **(PTZ)$_2$-Pt(bpy)-C$_{60}$′** (Figure 2), the

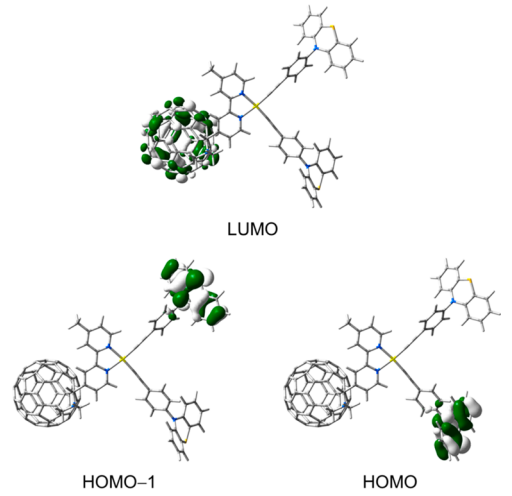

Figure 2. Spatial plots (isovalue = 0.03) of selected molecular orbitals of **(PTZ)$_2$-Pt(bpy)-C$_{60}$′** obtained from PBE0/CPCM calculation.

HOMO and HOMO−1 are localized on the Pt—C≡C—Ph units and phenothiazine entities, respectively. On the other hand, the lowest unoccupied molecular orbital (LUMO) of **(Ph)$_2$-Pt(bpy)** and **(PTZ)$_2$-Pt(bpy)** correspond to the π^* orbital of the bipyridine ligand, whereas the LUMO for **(Ph)$_2$-Pt(bpy)-C$_{60}$′** and **(PTZ)$_2$-Pt(bpy)-C$_{60}$′** is the π^* orbital localized on the C_{60} moiety.

The first two transitions computed at 432 and 475 nm for **(Ph)$_2$-Pt(bpy)** are the LLCT/MLCT [π(C≡C—Ph)/dπ(Pt) → π^*(bpy)] transitions (Table S1, Supporting Information). Selected singlet−singlet transitions for the other complexes are also listed in Table S1 (Supporting Information). For **(PTZ)$_2$-Pt(bpy)**, the first two transitions contain the LLCT [π(PTZ) → π^*(bpy)] character and are computed to be less intense, while the more intense LLCT/MLCT [π(C≡C—Ph—PTZ)/dπ(Pt) → π^*(bpy)] transitions are computed at 416 and 455 nm. These results further support the assignment of an origin of LLCT/MLCT character of the low-energy absorption band in the visible region. Several transitions (from $S_0 \rightarrow S_1$ to $S_0 \rightarrow S_4$) at 575−624 nm for **(Ph)$_2$-Pt(bpy)-C$_{60}$′** are the IL $\pi-\pi^*$ transitions of the C_{60}, which is in agreement with the low-energy absorption tail observed in the electronic absorption spectrum. Different from **(Ph)$_2$-Pt(bpy)-C$_{60}$′**, the S_1 and S_2 excited states for **(PTZ)$_2$-Pt(bpy)-C$_{60}$′** has LLCT [π(PTZ) → $\pi^*(C_{60})$] character. When compared with **(Ph)$_2$-Pt(bpy)** and **(PTZ)$_2$-Pt(bpy)**, the LLCT[π(C≡C—Ph—PTZ/Ph) → π^*(bpy)]/MLCT[dπ(Pt) → π^*(bpy)] transitions for **(Ph)$_2$-**

dx.doi.org/10.1021/ja5040073 | J. Am. Chem. Soc. 2014, 136, 10041−10052

Pt(bpy)-C_{60}′ and **$(PTZ)_2$-Pt(bpy)-C_{60}′** are found to be red-shifted (Table S1, Supporting Information).

Upon photoexcitation, **$(Ph)_2$-Pt(bpy)** displays observable emission in deaerated CH_2Cl_2 (Figure 3). The emission band

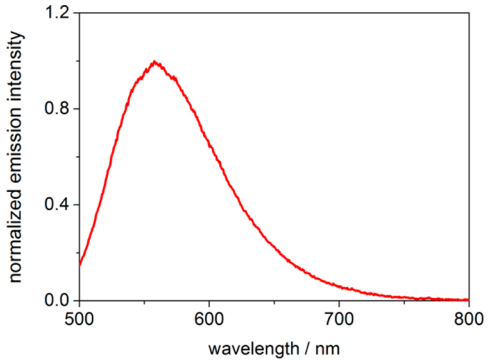

Figure 3. Normalized emission spectrum of **$(Ph)_2$-Pt(bpy)** in deaerated CH_2Cl_2.

observed in **$(Ph)_2$-Pt(bpy)** is of ^{3}MLCT/LLCT origin.[11a,b] However, the other platinum(II) complexes, **$(PTZ)_2$-Pt(bpy)-C_{60}**, **$(^t$BuPTZ$)_2$-Pt(bpy)-C_{60}**, **$(PTZ)_2$-Pt(bpy)**, **$(^t$BuPTZ$)_2$-Pt(bpy)** and **$(Ph)_2$-Pt(bpy)-C_{60}**, are nonemissive under identical conditions. The nonemissive nature of the phenothiazine- and/or fullerene-containing complexes may possibly be due to the occurrence of a quenching process in the excited state. A possible interpretation of this is that a competitive process of photoinduced electron transfer that leads to photochemical charge separation has taken place.

Electrochemistry. Cyclic voltammetry was carried out in 0.1 M *n*-Bu_4NPF_6 solution in deaerated dichloromethane. As expected, the first oxidation couple observed is the oxidation of the donor moiety (i.e., PTZ or ^{t}BuPTZ) and the introduction of the di-*tert*-butyl groups onto the 3,7-positions of phenothiazine would lower the potentials for oxidation by as much as 180 mV. On the other hand, the first and second reduction couples are the reductions of C_{60}, and the third reduction wave is the reduction of bipyridine ligand. The attachment of the C_{60} group to a platinum(II) bipyridine has been found to significantly affect the unoccupied orbitals of both groups. The $C_{60}/C_{60}^{\bullet-}$ reduction is shifted anodically by 50−60 mV in **$(Ph)_2$-Pt(bpy)-C_{60}**, **$(PTZ)_2$-Pt(bpy)-C_{60}** and **$(^t$BuPTZ$)_2$-Pt(bpy)-C_{60}** when compared to that of **di-^{t}BuPhC$_{60}$**, while the Pt(bpy)/Pt(bpy$^{\bullet-}$) reduction is shifted anodically by 20−50 mV compared to that of **$(Ph)_2$-Pt(bpy)**. The reduction potentials of the investigated compounds are summarized in Table 1 and the cyclic voltammograms of **$(^t$BuPTZ$)_2$-Pt(bpy)** and **$(^t$BuPTZ$)_2$-Pt(bpy)-C_{60}** are shown in Figure 4.

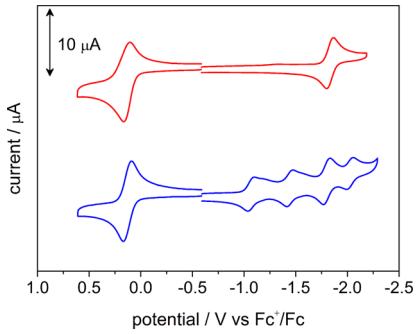

Figure 4. Cyclic voltammograms of **$(^t$BuPTZ$)_2$-Pt(bpy)** (top) and **$(^t$BuPTZ$)_2$-Pt(bpy)-C_{60}** (bottom) in CH_2Cl_2 containing 0.10 M *n*-Bu_4NPF_6 at 298 K.

From the observed reduction potentials given in Table 1, the free-energy changes associated with the CS and CR processes for **$(Ph)_2$-Pt(bpy)-C_{60}**, **$(PTZ)_2$-Pt(bpy)**, **$(^t$BuPTZ$)_2$-Pt(bpy)**, **$(PTZ)_2$-Pt(bpy)-C_{60}** and **$(^t$BuPTZ$)_2$-Pt(bpy)-C_{60}** can be estimated and are given in Table 2. These values include the corrections of the Coulombic interactions between the centers of positive and negative charges, with the distances *R* obtained from the optimized structure of **$(PTZ)_2$-Pt(bpy)-C_{60}**′ by DFT calculation (Table 3). It is interesting to note that two center-to-center distances between the donor and C_{60} (R_{D-C60}) are obtained, with the donor group farther away from the C_{60} referred to as *trans*- while the other as *cis*-. As R_{D-C60}, in each form, differs by ca. 4 Å, the Coulombic interaction of the ion-pair is very different, and the driving forces for charge separation in the *trans*- form are lowered by 0.03 eV, i.e., ΔG(CS) less negative by 0.03 eV. The energy difference of the ^{3}MLCT/LLCT excited state and the ground state (E_{00}) is estimated from the intersection of the emission and excitation spectra of **$(Ph)_2$-Pt(bpy)** measured at room temperature in deaerated dichloromethane, and is estimated to be 2.55 eV.

Table 1. Standard Potentials (vs Fc^+/Fc, in V)[a] of $(PTZ)_2$-Pt(bpy)-C_{60} and $(^t$BuPTZ$)_2$-Pt(bpy)-C_{60}, and Their Model Compounds PTZC_6H_4—C≡C—Ph, ^{t}BuPTZC_6H_4—C≡C—Ph, $(Ph)_2$-Pt(bpy), $(PTZ)_2$-Pt(bpy), $(^t$BuPTZ$)_2$-Pt(bpy), $(Ph)_2$-Pt(bpy)-C_{60} and di-^{t}BuPhC_{60}, in CH_2Cl_2

	E°/ V (vs Fc^+/Fc) in CH_2Cl_2			
molecule	$D^{\bullet+}/D$	$C_{60}/C_{60}^{\bullet-}$	$C_{60}^{\bullet-}/C_{60}^{2-}$	Pt(bpy)/Pt(bpy$^{\bullet-}$)
PTZC_6H_4—C≡C—Ph	+0.31	–	–	–
^{t}BuPTZC_6H_4—C≡C—Ph	+0.18	–	–	–
$(Ph)_2$-Pt(bpy)	–	–	–	−1.85
di-^{t}BuPhC_{60}	–	−1.13	−1.51	–
$(PTZ)_2$-Pt(bpy)	+0.27	–	–	−1.83
$(^t$BuPTZ$)_2$-Pt(bpy)	+0.13	–	–	−1.83
$(Ph)_2$-Pt(bpy)-C_{60}	$(+1.40)^{b,c}$	−1.08	−1.45	−1.82
$(PTZ)_2$-Pt(bpy)-C_{60}	+0.31	−1.07	−1.45	−1.80
$(^t$BuPTZ$)_2$-Pt(bpy)-C_{60}	+0.13	−1.07	−1.44	−1.80

[a]The standard potentials were determined as $E^\circ = (E^\circ_{pa} + E^\circ_{pc})/2$ by cyclic voltammetry in CH_2Cl_2 using *n*-Bu_4NPF_6 (0.1 M) as supporting electrolyte; scan rate = 100 mV s^{-1}. [b]Irreversible wave; E°_{pa} is reported. [c]A mixed platinum(II)/alkynyl-centered oxidation process.

dx.doi.org/10.1021/ja5040073 | J. Am. Chem. Soc. 2014, 136, 10041−10052

Table 2. Free-Energy Changes ΔG (eV) for Electron Transfer Reactions in CH_2Cl_2 Calculated from the Electrochemical Potentials after Correction for the Coulomb Interaction between the Charges[a]

reaction	ΔG(CS)/eV	ΔG(CR)/eV
$^3[(Ph)_2\text{-Pt(bpy)}]^*\text{-}C_{60} \rightarrow [(Ph)_2\text{-Pt}]^{\bullet+}\text{(bpy)-}C_{60}^{\bullet-}$	−0.23	−2.32
$(PTZ)_2\text{-}^3\text{Pt(bpy)}^* \rightarrow (PTZ)_2^{\bullet+}\text{-Pt(bpy)}^{\bullet-}$	−0.61	−1.94
$(^t\text{BuPTZ})_2\text{-}^3\text{Pt(bpy)}^* \rightarrow (^t\text{BuPTZ})_2^{\bullet+}\text{-Pt(bpy)}^{\bullet-}$	−0.75	−1.80
$(PTZ)_2\text{-}^3\text{Pt(bpy)}^*\text{-}C_{60} \rightarrow (PTZ)_2^{\bullet+}\text{-Pt(bpy)}^{\bullet-}\text{-}C_{60}$	−0.60	−1.95
$(PTZ)_2^{\bullet+}\text{-Pt(bpy)}^{\bullet-}\text{-}C_{60} \rightarrow (PTZ)_2^{\bullet+}\text{-Pt(bpy)-}C_{60}^{\bullet-}$	−0.73 (−0.70)[b]	−1.22 (−1.25)[b]
$(PTZ)_2\text{-}^3\text{Pt(bpy)}^*\text{-}C_{60} \rightarrow (PTZ)_2\text{-Pt(bpy)}^{\bullet+}\text{-}C_{60}^{\bullet-}$	−0.25	−2.30
$(PTZ)_2\text{-Pt(bpy)}^{\bullet+}\text{-}C_{60}^{\bullet-} \rightarrow (PTZ)_2^{\bullet+}\text{-Pt(bpy)-}C_{60}^{\bullet-}$	−1.08 (−1.05)[b]	−1.22 (−1.25)[b]
$(^t\text{BuPTZ})_2\text{-}^3\text{Pt(bpy)}^*\text{-}C_{60} \rightarrow (^t\text{BuPTZ})_2^{\bullet+}\text{-Pt(bpy)}^{\bullet-}\text{-}C_{60}$	−0.78	−1.77
$(^t\text{BuPTZ})_2^{\bullet+}\text{-Pt(bpy)}^{\bullet-}\text{-}C_{60} \rightarrow (^t\text{BuPTZ})_2^{\bullet+}\text{-Pt(bpy)-}C_{60}^{\bullet-}$	−0.68 (−0.65)[b]	−1.09 (−1.12)[b]
$(^t\text{BuPTZ})_2\text{-}^3\text{Pt(bpy)}^*\text{-}C_{60} \rightarrow (^t\text{BuPTZ})_2\text{-Pt(bpy)}^{\bullet+}\text{-}C_{60}^{\bullet-}$	−0.24	−2.31
$(^t\text{BuPTZ})_2\text{-Pt(bpy)}^{\bullet+}\text{-}C_{60}^{\bullet-} \rightarrow (^t\text{BuPTZ})_2^{\bullet+}\text{-Pt(bpy)-}C_{60}^{\bullet-}$	−1.22 (−1.19)[b]	−1.09 (−1.12)[b]

[a] $\Delta G(CR) = E^\circ$(anion red.) − E°(cation ox.) + $e/4\pi\varepsilon_0\varepsilon_s R_{DA}$ is for charge-recombination where R_{DA} is the charge-separation distance determined from DFT (Table 3); $\Delta G(CS) = -\Delta G(CR) - E_{00}$ is the driving force for charge-separation where E_{00} is estimated from the intersection of the emission and excitation spectra of **$(Ph)_2$-Pt(bpy)** measured at room temperature in deaerated dichloromethane, and is estimated to be 2.55 eV. The parameters used are $\varepsilon_0 = 8.85$, $\varepsilon_s = 8.93$ for CH_2Cl_2. [b] Driving forces for radical ion-pairs in *trans*-position.

Table 3. Center-to-Center Distances (Å)[a] between Various Moieties of $(PTZ)_2$-Pt(bpy)-C_{60}′

	center-to-center distance/Å			
	R_{Pt-C60}	R_{D-Pt}	R_{D-C60} (*trans*)	R_{D-C60} (*cis*)
$(PTZ)_2$-Pt(bpy)-C_{60}′	9.80	10.19	19.16	15.00

[a] The center-to-center distance is measured from the centroid of the moieties.

Transient Absorption Spectroscopy. Femtosecond transient absorption spectroscopy was used to investigate the photoinduced electron transfer reactions in **$(Ph)_2$-Pt(bpy)-C_{60}**, **$(PTZ)_2$-Pt(bpy)-C_{60}** and **$(^t$BuPTZ$)_2$-Pt(bpy)-C_{60}** and the resulting spectra have been subjected to global fitting with a sequential model to yield evolution-associated difference spectra (EADS) and with a parallel model to yield decay-associated difference spectra (DADS).[15] In general, laser-irradiation of complexes at 400 nm in dichloromethane initially populates ca. 60% of the ^{1}MLCT/LLCT excited state and ca. 40% of the $^1C_{60}$ excited state, based on the absorption of the related model compounds, **$(Ph)_2$-Pt(bpy)** and **di-^{t}BuPhC_{60}** (Figure 1). Intersystem crossing (ISC) of the ^{1}MLCT/LLCT excited state occurs subsequently within the instrumental response time with a time constant of $\tau < 150$ fs to produce the ^{3}MLCT/LLCT excited state, consistent with that of a related Pt(II) bipyridine complex.[11a,b] The first resolved EADS component for all complexes therefore is the combination of the ^{3}MLCT/LLCT and $^1C_{60}$ excited states, characterized by the unstructured absorption between 550 and 700 nm (λ_{max} = 650 nm) associated with the ^{3}MLCT/LLCT excited state,[11a,b] and

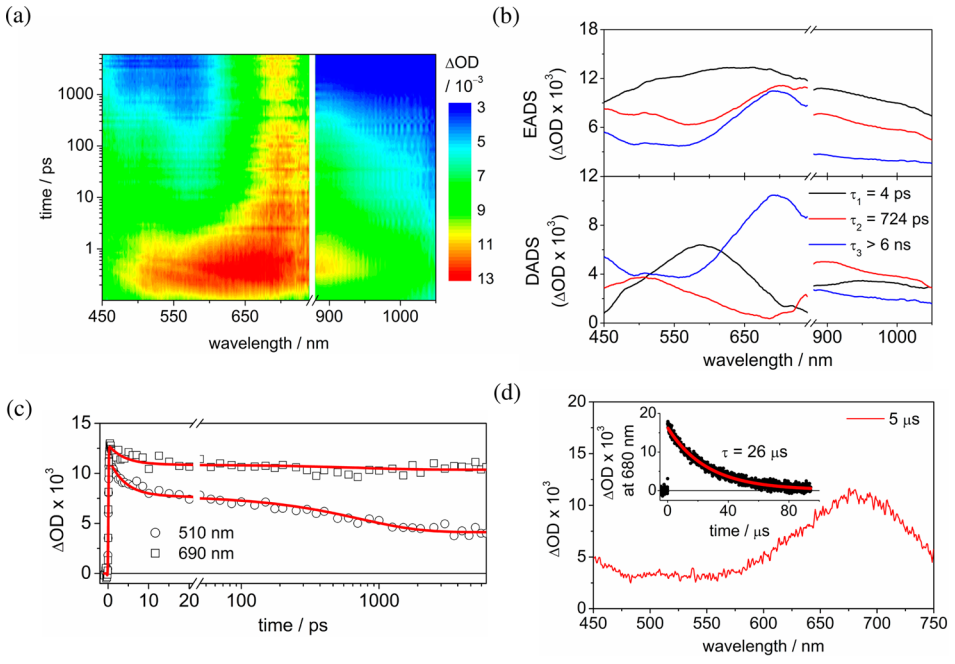

Figure 5. Transient absorption difference spectra of **$(Ph)_2$-Pt(bpy)-C_{60}** following excitation at 400 nm in CH_2Cl_2: (a) contour plot of the spectroscopic responses following femtosecond laser pulse irradiation; (b) EADS (top) and DADS (bottom) derived from the global analysis; (c) time decay profiles of optical density at 510 and 690 nm; and (d) taken at 5 μs after nanosecond laser pulse excitation at 355 nm in deaerated CH_2Cl_2, with time-decay profile of optical density at 680 nm (inset).

dx.doi.org/10.1021/ja5040073 | J. Am. Chem. Soc. 2014, 136, 10041−10052

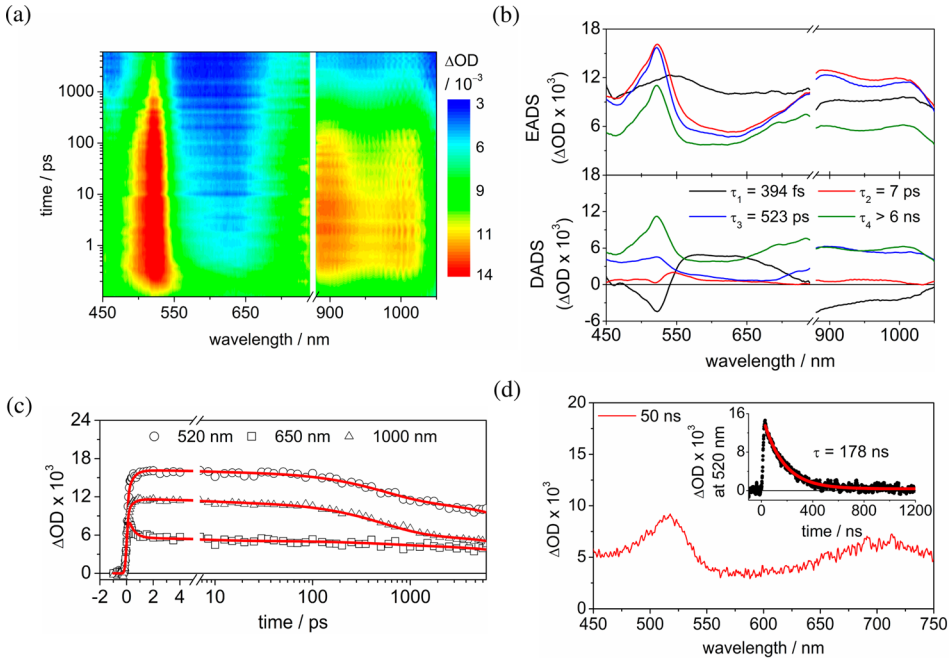

Figure 6. Transient absorption difference spectra of $(\mathbf{PTZ})_2$-**Pt(bpy)-C$_{60}$** following excitation at 400 nm in CH_2Cl_2: (a) contour plot of the spectroscopic responses following femtosecond laser pulse irradiation; (b) EADS (top) and DADS (bottom) derived from the global analysis; (c) time decay profiles of optical density at 520, 650 and 1000 nm; and (d) taken at 50 ns after nanosecond laser pulse excitation at 355 nm in deaerated CH_2Cl_2, with time-decay profile of optical density at 520 nm (inset).

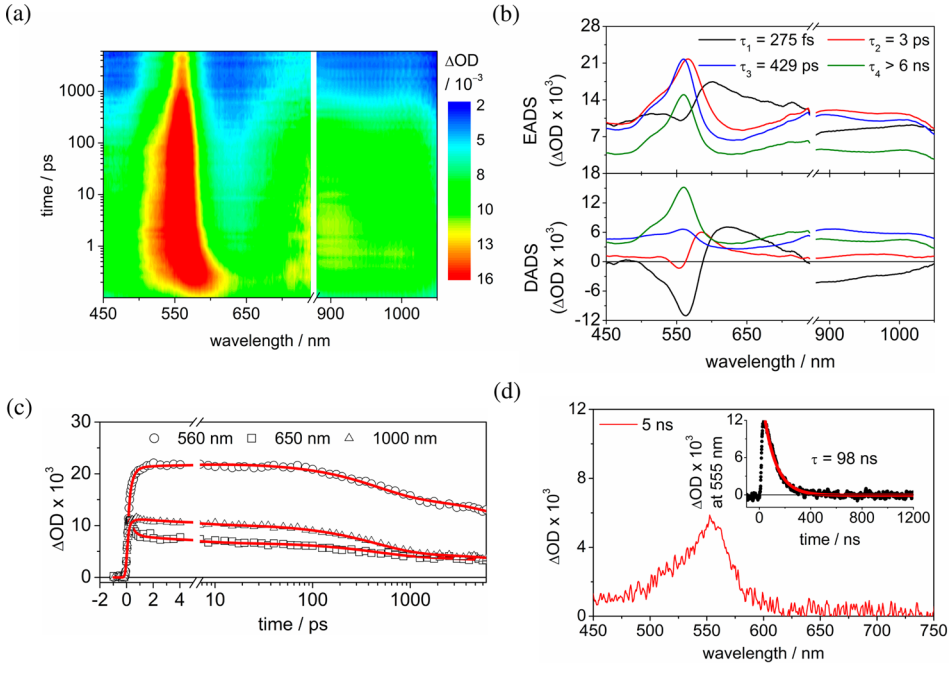

Figure 7. Transient absorption difference spectra of $(^t\mathbf{BuPTZ})_2$-**Pt(bpy)-C$_{60}$** following excitation at 400 nm in CH_2Cl_2: (a) contour plot of the spectroscopic responses following femtosecond laser pulse irradiation; (b) EADS (top) and DADS (bottom) derived from the global analysis; (c) time decay profiles of optical density at 560, 650 and 1000 nm; and (d) taken at 5 ns after nanosecond laser pulse excitation at 355 nm in deaerated CH_2Cl_2, with time-decay profile of optical density at 555 nm (inset).

the absorption at λ_{max} = 510 and 890 nm of the localized $^1C_{60}$* (Figures 5–7).[13b]

For **(Ph)$_2$-Pt(bpy)-C$_{60}$**, the ^{3}MLCT/LLCT excited state undergoes triplet–triplet (T–T) energy transfer to C_{60} at τ_1 = 4 ps, confirmed by the presence of $^3C_{60}$* with characteristic absorption at λ_{max} = 690 nm[12c,e,13b,16] in the second EASD component. This component also shows the coexistence of $^1C_{60}$* which decays after 724 ps through ISC to produce the final component of $^3C_{60}$* with characteristic absorption at λ_{max} = 690 nm.[12c,e,13b,16] The ISC rate of $^1C_{60}$* is close to that found for **di-^{t}BuPhC$_{60}$** of ~1000 ps (Figure S4, Supporting Information). The remaining long-lived $^3C_{60}$* state eventually decays with a lifetime τ = 26 μs (Figure 5d), in good agreement

dx.doi.org/10.1021/ja5040073 | J. Am. Chem. Soc. 2014, 136, 10041–10052

Scheme 2. Schematic Energy Diagrams for Photoinduced Energy and Charge Transfer of (a) $(Ph)_2$-Pt(bpy)-C_{60}, (b) $(PTZ)_2$-Pt(bpy)-C_{60} and (^{t}BuPTZ)$_2$-Pt(bpy)-C_{60} in CH_2Cl_2[a,b]

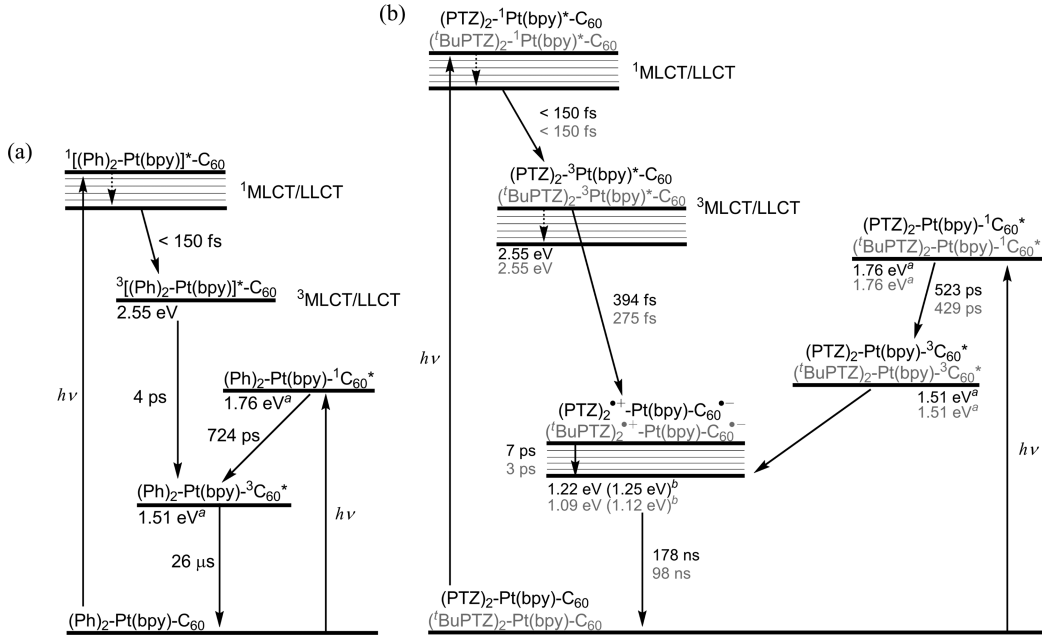

[a]Energies of $^1C_{60}$* and $^3C_{60}$* excited states are obtained from ref 12e. [b]Energy for radical ion-pairs in *trans*-position.

Table 4. Observed Reaction Rates of Energy-Transfer (k_{EnT}), Intersystem Crossing of $^1C_{60}$* (k_{ISC}), Charge-Separation (k_{CS}), Vibrational Relaxation (k_{VR}), Charge-Recombination (k_{CR}) and Relaxation of $^3C_{60}$* (k_T) for di-^{t}BuC$_{60}$, $(Ph)_2$-Pt(bpy)-C_{60}, $(PTZ)_2$-Pt(bpy), (^{t}BuPTZ)$_2$-Pt(bpy), $(PTZ)_2$-Pt(bpy)-C_{60} and (^{t}BuPTZ)$_2$-Pt(bpy)-C_{60}

molecule	k_{EnT}/s^{-1}	k_{ISC}/s^{-1}	k_{CS}/s^{-1}	k_{VR}/s^{-1}	k_{CR}/s^{-1}	k_T/s^{-1}
di-^{t}BuC$_{60}$	–	9.1×10^9	–	–	–	4.2×10^4
$(Ph)_2$-Pt(bpy)-C_{60}	2.5×10^{11}	1.4×10^9	–	–	–	3.8×10^4
$(PTZ)_2$-Pt(bpy)	–	–	6.3×10^{11}	2.1×10^{10}	4.8×10^8	–
(^{t}BuPTZ)$_2$-Pt(bpy)	–	–	1.2×10^{12}	4.4×10^{10}	4.4×10^8	–
$(PTZ)_2$-Pt(bpy)-C_{60}	–	1.9×10^9	2.5×10^{12}	1.4×10^{11}	5.6×10^6	–
(^{t}BuPTZ)$_2$-Pt(bpy)-C_{60}	–	2.3×10^9	3.6×10^{12}	3.0×10^{11}	1.0×10^7	–

with that of **di-^{t}BuPhC$_{60}$** (τ = 24 μs, Figure S5, Supporting Information).

It should be noted that charge separation through an electron transfer reaction from the ^{3}MLCT/LLCT excited state to C_{60} generating $[(Ph)_2\text{-Pt}]^{•+}$(bpy)-$C_{60}^{•−}$ is energetically accessible (ΔG(CS) = −0.23 eV, Table 2), but this component with the well-established $C_{60}^{•−}$ absorption at about 1000 nm[2a,13b,16] was not found, indicating that the CS state is not populated. Analogous results have been obtained in the related Ru(bpy)$_3^{2+}$-C_{60} complexes.[12d]

$(PTZ)_2$-Pt(bpy)-C_{60} and **(^{t}BuPTZ)$_2$-Pt(bpy)-C_{60}** behave differently when compared with their related dyad **$(Ph)_2$-Pt(bpy)-C_{60}** upon photoexcitation at 400 nm in dichloromethane. The EADS and DADS of the four resolved components are shown in Figures 6b and 7b. The first component depicts the initial formation of the ^{3}MLCT/LLCT excited state. This is followed by charge transfer process to produce the CS species, namely, $(PTZ)_2^{•+}$-Pt(bpy)-$C_{60}^{•−}$ and (^{t}BuPTZ)$_2^{•+}$-Pt(bpy)-$C_{60}^{•−}$, with rise time τ_1 = 394 and 275 fs, respectively (vide infra). This component is characterized by strong absorption features at ca. 520 nm for $PTZ^{•+}$ or ca. 560 nm for ^{t}BuPTZ$^{•+}$,[8b,14a,d,16,17] as well as the $C_{60}^{•−}$ absorption at ca. 1000 nm.[2a,13b,16] As vibrational relaxation of the ^{3}MLCT/LLCT excited state has not yet been completed until ~4 ps,[11b] the charge transfer from a vibrationally unrelaxed ^{3}MLCT/LLCT excited state is possible[18] and the subsequent vibrational relaxation of the CS state, identified by the blue-shifting of peak maxima as well as the narrowing of the spectral bands,[19] occurs at a time τ_2 = 7 ps for **$(PTZ)_2$-Pt(bpy)-C_{60}** and 3 ps for **(^{t}BuPTZ)$_2$-Pt(bpy)-C_{60}**. As the charge transfer process is exceptionally fast, much faster than that of the T−T energy transfer process (τ = 4 ps for **$(Ph)_2$-Pt(bpy)-C_{60}**), the formation of $(PTZ)_2^{•+}$-Pt(bpy)-$C_{60}^{•−}$ and (^{t}BuPTZ)$_2^{•+}$-Pt(bpy)-$C_{60}^{•−}$ is very efficient with quantum yields ($\Phi_{CS(MLCT/LLCT)}$) estimated to be 0.91 and 0.94, respectively (Supporting Information Section S3). From the decay profiles at 520 nm for **$(PTZ)_2$-Pt(bpy)-C_{60}** and 555 nm for **(^{t}BuPTZ)$_2$-Pt(bpy)-C_{60}**, the lifetimes of the CS states are determined to be 178 and 98 ns (Figures 6d and 7d). Notably, $^1C_{60}$* is also observed in the resolved component spectra, which undergoes ISC to form $^3C_{60}$* with time constants τ_3 = 523 ps for **$(PTZ)_2$-Pt(bpy)-C_{60}** and τ_3 = 429 ps for **(^{t}BuPTZ)$_2$-Pt(bpy)-C_{60}**. The absorption of $^3C_{60}$* is also observed in the transient absorption difference spectrum of **$(PTZ)_2$-Pt(bpy)-C_{60}** taken at 50 ns (Figure 6d), and the time decay profile at 680 nm (not presented) obeys the first-order kinetics with a lifetime of 178 ns, identical to that of the 520 nm absorption. Unambiguously, the $^3C_{60}$* state eventually decays

dx.doi.org/10.1021/ja5040073 | J. Am. Chem. Soc. 2014, 136, 10041−10052

to the ground state via the energetically lower-lying CS state, $(PTZ)_2^{\bullet+}$-Pt(bpy)-$C_{60}^{\bullet-}$. Furthermore, due to the large energy gap between the CS state and the $^3C_{60}$* state (ΔG(CS) − $\Delta G(^3C_{60}*)$ = 0.29 eV), from the Boltzmann distribution, the CS state is largely populated at the equilibrium and the direct relaxation rate of the CS state is equal to the observed CR rate (τ_{CR} = 178 ns or $k_{CR} = 5.6 \times 10^6$ s^{-1}), with essentially no delay due to the slow relaxation of the $^3C_{60}$* state.[20] By assuming the ISC of ^{1}MLCT/LLCT excited state is unity (i.e., $\Phi_{ISC(MLCT/LLCT)}$ = 1) and the quantum yield for the ISC of $^1C_{60}$* ($\Phi_{ISC(C60)}$) is 0.98,[21] and the total efficiencies for the formation of $(PTZ)_2^{\bullet+}$-Pt(bpy)-$C_{60}^{\bullet-}$ and $(^t$BuPTZ$)_2^{\bullet+}$-Pt-(bpy)-$C_{60}^{\bullet-}$ ($\Phi_{CS(total)}$) are both estimated to be 0.99 (Supporting Information Section S3).

The energetic and kinetic data for **(Ph)$_2$-Pt(bpy)-C$_{60}$**, **(PTZ)$_2$-Pt(bpy)-C$_{60}$** and **(^{t}BuPTZ)$_2$-Pt(bpy)-C$_{60}$** are summarized in Scheme 2, and the observed reaction rate constants are listed in Table 4. The reaction profiles of the triads clearly illustrate that the charge-separation process is in the Marcus normal region[22] as greater driving forces in **(^{t}BuPTZ)$_2$-Pt(bpy)-C$_{60}$** lead to faster reactions, while the charge-recombination process is in the inverted region[22] with slower reaction observed for **(PTZ)$_2$-Pt(bpy)-C$_{60}$**.

$$k_{ET} = \frac{2\pi}{\hbar} V^2 (4\pi\lambda k_B T)^{-1/2} \exp\left[\frac{-(\lambda + \Delta G^\circ)^2}{4\lambda k_B T}\right] \quad (1)$$

Ultrafast charge transfer reactions are also observed in the associated dyads, **(PTZ)$_2$-Pt(bpy)** and **(^{t}BuPTZ)$_2$-Pt(bpy)**, and their observed femtosecond transient absorption spectra and EADS are shown in Figures S6 and S7 (Supporting Information). The revealed CS process from ^{3}MLCT/LLCT excited state occurred at τ = 2 ps for **(PTZ)$_2$-Pt(bpy)** and τ = 814 fs for **(^{t}BuPTZ)$_2$-Pt(bpy)**. According to the rate equation for nonadiabatic electron transfer (eq 1),[22] the rate for the reaction k_{ET} depends on the electronic coupling term (V), the driving force (ΔG°) and the total reorganization energy (λ). The electron delocalization in the ^{3}MLCT/LLCT excited state in fact reduces the reorganization energy and enhances the electronic coupling, both of which would lead to a more efficient charge transfer.[23] Forward charge transfer reactions in **(PTZ)$_2$-Pt(bpy)** and **(^{t}BuPTZ)$_2$-Pt(bpy)** are ~250−500 times faster than that of the structurally similar but nonconjugated platinum(II) bipyridine bis(phenothiazine alkynyl) system with a methylene bridge between the Pt—C≡C—Ph and the PTZ units,[8b] for which the observed lifetime is on the order of hundreds of picoseconds. The driving forces for the charge-transfer reaction are determined to be −0.61 eV for **(PTZ)$_2$-Pt(bpy)** and −0.75 eV for **(^{t}BuPTZ)$_2$-Pt(bpy)** (Table 2), much larger than that of the nonconjugated system (ΔG(CS) = −0.34 eV).[8b] Therefore, the electron transfer reaction for a system in the Marcus normal region[22] should be accelerated. More importantly, the conjugation is preserved after the removal of the methylene bridge between the Pt—C≡C—Ph and the PTZ units, and therefore enhanced electronic coupling with the adjacent PTZ donor is provided to mediate the charge-transfer process. Similarly, a slower charge transfer rate is observed in a PTZ-Pt(bpy)-MNDI complex, in which the electronic coupling between the PTZ and the Pt—C≡C—Ph units is minimized by restricting the rotation of the additional phenyl ring adjacent to the PTZ and the phenyl ring on the Pt—C≡C—Ph unit.[14d] On the other hand, in the CS state of **(PTZ)$_2$-Pt(bpy)** and **(^{t}BuPTZ)$_2$-Pt(bpy)**, the charges are well separated at a distance of 10 Å (see R_{D-Pt} for **(PTZ)$_2$-Pt(bpy)-C$_{60}$′** in Table 3) and are entirely localized onto the phenothiazine and bipyridine moieties (see HOMO and LUMO in Figure S2, Supporting Information). Therefore, the donor−acceptor electronic coupling is sufficiently weak, and hence the CR process has a lifetime of 2 ns which is comparable to the 5 ns obtained for the nonconjugated system.[8b] The slow CR process is also attributed to the difference in spin multiplicity between the CS state and the ground state.

Moreover, the charge-separation of **(PTZ)$_2$-Pt(bpy)-C$_{60}$** and **(^{t}BuPTZ)$_2$-Pt(bpy)-C$_{60}$** from the ^{3}MLCT/LLCT excited state can, in principle, occur via two alternative mechanisms, namely, reductive quenching (eq 2) and oxidative quenching (eq 3):

$$\begin{aligned}&(PTZ)_2\text{-}{}^3\text{Pt(bpy)*-}C_{60}\\ &\rightarrow (PTZ)_2^{\bullet+}\text{-Pt(bpy)}^{\bullet-}\text{-}C_{60}\\ &\rightarrow (PTZ)_2^{\bullet+}\text{-Pt(bpy)-}C_{60}^{\bullet-}\end{aligned} \quad (2)$$

$$\begin{aligned}&(PTZ)_2\text{-}{}^3\text{Pt(bpy)*-}C_{60}\\ &\rightarrow (PTZ)_2\text{-Pt}^{\bullet+}\text{(bpy)-}C_{60}^{\bullet-}\\ &\rightarrow (PTZ)_2^{\bullet+}\text{-Pt(bpy)-}C_{60}^{\bullet-}\end{aligned} \quad (3)$$

As reductive quenching (eq 2) and oxidative quenching (eq 3) are energetically accessible, i.e., ΔG < 0 eV (Table 2), both pathways are expected to be observed. However, the associated dyad **(Ph)$_2$-Pt(bpy)-C$_{60}$** illustrates no electron transfer from the ^{3}MLCT/LLCT excited state to the C_{60} unit, suggesting the oxidative quenching mechanism (eq 3) is not likely. On the other hand, reductive quenching has been observed in **(PTZ)$_2$-Pt(bpy)** and **(^{t}BuPTZ)$_2$-Pt(bpy)**, and thus charge separation in the triads should occur via the reductive quenching mechanism (eq 2). As the primary CS state, $(PTZ)_2^{\bullet+}$-Pt(bpy)$^{\bullet-}$-C_{60} and $(^t$BuPTZ$)_2^{\bullet+}$-Pt(bpy)$^{\bullet-}$-C_{60}, cannot be observed in both triads, the subsequent electron transfer reaction should be enormously fast such that the detection of the primary CS state becomes impossible. The ultrafast electron transfer from the bipyridine unit to the C_{60} unit is attributed to the strong coupling between the bipyridine and the C_{60} moieties, in which the two units are connected in close proximity, and such a strong coupling is also observed in directly linked porphyrin/phytochlorin-C_{60}[24] and ferrocene-porphyrin systems,[25] which also lead to efficient charge transfers. Because of the strong coupling, the electron transfer reaction is likely to be mediated by tunneling via the through-space mechanism or by superexchange in the through-bond mechanism.[26] On the other hand, with regard to the ultrafast CS process in the triads, the CR process is relatively slow, with 5-orders of magnitude slower than the CS process (Table 4). As the charges are separated by 15 Å for the *cis*- or 20 Å for the *trans*- system, the donor−acceptor coupling is significantly reduced, which slows down the CR process. The difference in spin multiplicity between the CS state and the ground state would also slow down the CR process significantly.

CONCLUSION

The photoinduced electron transfer reactions of donor−chromophore−C_{60} triads, **(PTZ)$_2$-Pt(bpy)-C$_{60}$** and **(^{t}BuPTZ)$_2$-Pt(bpy)-C$_{60}$**, along with their associated dyad **(Ph)$_2$-Pt(bpy)-C$_{60}$**, were studied using the femtosecond and nanosecond transient absorption spectroscopy. **(Ph)$_2$-Pt(bpy)-C$_{60}$** shows ultrafast picosecond T−T energy transfer from the

dx.doi.org/10.1021/ja5040073 | J. Am. Chem. Soc. 2014, 136, 10041−10052

^{3}MLCT/LLCT excited state to C_{60}, and the resulting long-lived $^3C_{60}$* state decays to the ground state in microsecond time scale. Through the direct attachment of the electron donor to the chromophore and short spatial distances between the chromophore and the donor/acceptor, both triads show ultrafast femtosecond charge separation with quantum yields of over 90% in which the charges are 15−20 Å apart; also, controlling the spin multiplicity of the CS state with the cooperation of a transition metal−ligand chromophore slows down the CR process.

EXPERIMENTAL SECTION

General Methods. ^{1}H NMR spectra were recorded on a Bruker AVANCE 300 (300 MHz) or Bruker AVANCE 400 (400 MHz) Fourier-transform NMR spectrometers with chemical shifts reported relative to tetramethylsilane (Me_4Si). Positive-ion FAB mass spectrometry were recorded on a Thermo Scientific DFS high-resolution magnetic sector mass spectrometer. Elemental analyses of the newly synthesized complexes were performed using a Flash EA 1112 elemental analyzer at the Institute of Chemistry, Chinese Academy of Sciences, Beijing. Ultraviolet−visible spectra were recorded on a Varian Cary 50 UV−vis spectrophotometer in spectroscopic grade CH_2Cl_2. Steady-state emission spectra were recorded on a Spex Fluorolog-3 Model FL3-211 spectrofluorometer equipped with a R2658P PMT detector. Measurements of the butyronitrile glass at 77 K were conducted with samples contained in a quartz tube inside a quartz-walled Dewar flask filled with liquid nitrogen. The concentrations of the complex solutions in butyronitrile for glass-emission measurements were in the range of 10^{-6} mol dm^{-3}. All solutions for photophysical studies were deaerated on a high-vacuum line in a two-compartment cell that consisted of a 10 mL Pyrex bulb and a 1 cm path length quartz cuvette and sealed against the atmosphere by a Bibby Rotaflo HP6 Teflon stopper. The solutions were rigorously degassed with at least four successive freeze−pump−thaw cycles.

Electrochemical Measurements. The cyclic voltammetry measurements were performed on a CHI 620A electrochemical analyzer in deaerated dichloromethane containing 0.10 M n-Bu_4NPF_6 as supporting electrolyte at 298 K. A glassy carbon working electrode was polished with Linde polishing alumina suspension and rinsed with deionized water followed by dichloromethane before use. A platinum wire was used as a counter electrode and an $Ag/AgNO_3$ (0.1 M in acetonitrile) was used as a reference electrode. All experiments were followed by the addition of ferrocene, and the ferrocene/ferricenium redox potential was used as an internal reference.

Transient Absorption (TA) Measurements. The fs time-resolved experiments were performed based on a commercial Ti:sapphire regenerative amplifier laser system and home-built TA spectrometers.[27] The sample solutions were excited by a 400 nm pump laser; the subsequent excited state processes taking place on fs to several ns time-scale were detected by a second probe pulse induced by an 800 nm laser in the TA method. The 400 nm pump laser was the second harmonic of the 800 nm fundamental (1 kHz repetition rate, ∼35 fs duration) produced with a BBO crystal. In the fs-TA experiments, the excited states were probed by a white light continuum (WLC) pulse produced by focusing part of the 800 nm laser onto a rotating quartz plate. The TA signals were collected by a monochromator and detected with a thermoelectric cooled CCD detector. The spectral window for the TA covers 450−740 nm and 600−1050 nm regions. TA signals at wavelength from 740 to 880 nm were masked by the 800 nm fundamental and thus were not shown in the fs-TA in Figures 5−7 and Figures S4−S7 (Supporting Information). Temporal delay of the probe relative to pump pulse was controlled by an optical delay line in the fs-TA. The instrument response function (IRF) of our ultrafast system is wavelength-dependent. As the detection wavelength varies from 1050 to 450 nm, the IRF change from ∼150 to 250 fs. For the fs-TA spectra, corrections have been done to eliminate the wavelength-dependent time shift caused by the group velocity dispersion.

The fs-TA spectra were analyzed by global analysis[15] with the graphical interface program Glotaran[28] (http://glotaran.org/). The global analysis is based upon the fact that the observed TA data are a superposition of the spectroscopic properties of n_{comp} different components weighted by their concentration, and the time-resolved spectrum $\psi(t,\lambda)$ can be described as[15,28]

$$\psi(t,\lambda) = \sum_{i=1}^{n_{comp}} c_i(t)\varepsilon_i(\lambda) \tag{4}$$

where $c_i(t)$ and $\varepsilon_i(\lambda)$ are the concentration and spectrum of component i. The TA spectra are globally fitted with two different models: a parallel model and a sequential model. In the parallel model, which constitutes the decay-associated difference spectra (DADS), n_{comp} noninteracting components monoexponentially decay in parallel and can be described as[15,28]

$$\psi(t,\lambda) = \sum_{i=1}^{n_{comp}} c_i^{DADS}(t)\mathrm{DADS}_i(\lambda) \tag{5}$$

where $c_i^{DADS}(t) = \exp(-k_i t) \oplus i(t)$ is the exponentially decaying concentration of component i convolved with the IRF $i(t)$. In the sequential model, the associated spectra are called evolution-associated difference spectra (EADS) and can be described as[15,28]

$$\psi(t,\lambda) = \sum_{i=1}^{n_{comp}} c_i^{EADS}(t)\mathrm{EADS}_i(\lambda) \tag{6}$$

with $c_i^{EADS}(t) = \sum_{j=1}^{i} b_{ji} \exp(-kjt) \oplus i(t)$ and $b_{ji} = \prod_{m=1}^{i} k_m / \prod_{n=1,n\neq j}^{i} (k_n - k_j)$, where k_j is the decay rate of component j and the amplitudes b_{ji} of the exponential decays are defined for $j \leq i$ assuming $b_{11} = 1$.[15,28] The DADS are the change of absorption with a certain lifetime, while the EADS represent the spectral evolution with successively increasing lifetime.

Nanosecond transient absorption spectroscopy experiments were performed using an LP920-KS Laser Flash Photolysis Spectrometer (Edinburgh Instruments, Ltd., Livingston, UK) at ambient temperature. The excitation source was the 355 nm output (third harmonic) of an Nd:YAG laser (Spectra-Physics Quanta-Ray Lab-130 Pulsed Nd:YAG Laser) and the probe light source was a Xe900 450 W xenon arc lamp. The transient absorption spectra were detected using an image-intensified CCD camera (Andor) with PC plug-in controller, fully operated by L900 spectrometer software. The absorption kinetics were detected using a Hamamatsu R928 photomultiplier tube and recorded using a Tektronix Model TDS3012B (100 MHz, 1.25 GS s^{-1}) digital oscilloscope. Samples were freshly prepared and degassed with at least four freeze−pump−thaw cycles on a high-vacuum line in a two compartment cell that consisted of a 10 mL Pyrex bulb and a 1 cm path length quartz cuvette.

Computational Details. Calculations were carried out using Gaussian 09 software package.[29] The ground-state geometries of **(Ph)$_2$-Pt(bpy)**, **(PTZ)$_2$-Pt(bpy)**, **(Ph)$_2$-Pt(bpy)-C$_{60}$′** and **(PTZ)$_2$-Pt(bpy)-C$_{60}$′** were fully optimized by using the density functional theory (DFT) with hybrid Perdew, Burke, and Ernzerhof functional (PBE0).[30] Vibrational frequency calculations were performed for all stationary points to verify that each was a minimum (NIMAG = 0) on the potential energy surface. On the basis of the ground state optimized geometries, the time-dependent density functional theory (TDDFT)[31] at the same level of theory associated with the conductor-like polarizable continuum model (CPCM)[32] using CH_2Cl_2 as the solvent were employed to compute the singlet−singlet transitions for the complexes. For all the calculations, the Stuttgart effective core potentials (ECPs) and the associated basis set were applied to describe Pt[33] with f-type polarization functions (ζ = 0.993),[34] while the 6-31G(d,p) basis set[35] was used for all other atoms. The DFT and TDDFT calculations were performed with a pruned (99,590) grid.

Synthesis. 4-Methyl-2,2′-bipyridine-4′-carboxaldehyde,[36] *N*-dodecyl glycine,[37] and 3,7-di-*tert*-butylphenothiazine[38] were prepared

dx.doi.org/10.1021/ja5040073 | J. Am. Chem. Soc. 2014, 136, 10041−10052

according to literature procedures. The synthetic details of organic ligands and organic model compounds, **$PTZC_6H_4$—C≡C—Ph**, **$^tBuPTZC_6H_4$—C≡C—Ph** and **di-^{t}BuPhC$_{60}$**, are described in the Supporting Information.

General Procedure of Platinum Complexation. 4,4′-Dimethyl-2,2′-byipyridine/fullerene-appended bipyridine and $[PtCl_2(DMSO)_2]$ were stirred in dichloromethane, under N_2, for 15 h. The solvent was then reduced and diethyl ether was added. The resulting precipitate, dichloroplatinum(II) precursor, was filtered and dried. Dichloroplatinum(II) precursor and arylacetylene (2.5 equiv) were added in deaerated dichloromethane. Triethylamine (∼1 mL) was added, followed by the addition of copper iodide (∼2 mg). The reaction mixture was stirred at room temperature, under N_2, for 15 h. The reaction was filtered and the solvent was removed under reduced pressure. The product was purified by column chromatography on silica gel using chloroform-1% methanol as eluent, and then recrystallized from chloroform/diethyl ether.

(Ph)$_2$-Pt(bpy). (Yield: 85%). ^{1}H NMR (400 MHz, $C_2D_2Cl_4$, 90 °C): δ/ppm 9.63 (d, J = 5.2 Hz, 2H), 7.87 (s, 2H), 7.54 (d, J = 7.2 Hz, 4H), 7.40 (d, J = 4.9 Hz, 2H), 7.31 (t, J = 7.2 Hz, 4H), 7.20 (t, J = 7.2 Hz, 2H), 2.54 (s, 6H). FAB-MS (m/z): $[M + H]^+$ 582.2. Elemental analysis calcd (%) for $C_{28}H_{22}N_2Pt{\cdot}H_2O$: C 56.09, H 4.03, N 4.67. Found: C 56.12, H 3.81, N 4.75.

(PTZ)$_2$-Pt(bpy). (Yield: 82%). ^{1}H NMR (400 MHz, $CDCl_3$): δ/ppm 9.64 (d, J = 5.7 Hz, 2H), 8.14 (d, J = 7.7 Hz, 4H), 7.92 (s, 2H), 7.76 (d, J = 8.5 Hz, 4H), 7.43 (m, 14H), 7.28 (m, 4H), 2.55 (s, 6H). FAB-MS (m/z): $[M]^+$ 975.9. Elemental analysis calcd (%) for $C_{52}H_{36}N_4S_2Pt{\cdot}2H_2O$: C 61.71, H 3.98, N 5.54. Found: C 61.59, H 3.71, N 5.46.

(^{t}BuPTZ)$_2$-Pt(bpy). (Yield: 50%). ^{1}H NMR (400 MHz, $CDCl_3$): δ/ppm 9.57 (d, J = 5.7 Hz, 2H), 7.94 (s, 2H), 7.72 (d, J = 8.4 Hz, 4H), 7.38 (d, J = 5.1 Hz, 2H), 7.25 (d, J = 8.6 Hz, 4H), 7.04 (d, J = 2.2 Hz, 4H), 6.86 (dd, J = 8.6, 2.2 Hz, 4H), 6.22 (d, J = 8.6 Hz, 4H), 2.55 (s, 6H), 1.23 (s, 36H). FAB-MS (m/z): $[M]^+$ 1200.1. Elemental analysis calcd (%) for $C_{68}H_{68}N_4S_2Pt{\cdot}2H_2O$: C 66.05, H 5.87, N 4.53. Found: C 66.30, H 5.62, N 4.59.

(Ph)$_2$-Pt(bpy)-C$_{60}$. (Yield: 36%). ^{1}H NMR (400 MHz, $C_2D_2Cl_4$, 90 °C): δ/ppm 9.94 (d, J = 5.9 Hz, 1H), 9.70 (d, J = 5.5 Hz, 1H), 8.53 (s, 1H), 8.12 (bs, 1H), 7.91 (s, 1H), 7.52 (m, 4H), 7.46 (d, J = 5.8 Hz, 1H), 7.29 (m, 4H), 7.19 (m, 2H), 5.32 (s, 1H), 5.24 (d, J = 9.6 Hz, 1H), 4.33 (d, J = 9.6 Hz, 1H), 3.21 (m, 1H), 2.80 (m, 1H), 2.56 (s, 3H), 2.51 (m, 1H), 2.05 (m, 1H), 1.98 (m, 1H), 1.74 (m, 1H), 1.60 (m, 4H), 1.35 (bs, 12H), 0.95 (bs, 3H). FAB-MS (m/z): $[M - 2H]^+$ 1494.2. Elemental analysis calcd (%) for $C_{101}H_{47}N_3Pt{\cdot}3H_2O$: C 78.18, H 3.44, N 2.71. Found: C 78.03, H 3.22, N 2.88.

(PTZ)$_2$-Pt(bpy)-C$_{60}$. (Yield: 30%). ^{1}H NMR (400 MHz, $CDCl_3$, 50 °C): δ/ppm 9.95 (d, J = 5.7 Hz, 1H), 9.73 (d, J = 5.7 Hz, 1H), 8.54 (bs, 1H), 8.11 (bs, 1H), 7.95 (s, 1H), 7.74 (d, J = 8.2 Hz, 2H), 7.71 (d, J = 8.2 Hz, 2H), 7.46 (d, J = 5.2 Hz, 1H), 7.26 (d, J = 1.9 Hz, 2H), 7.24 (d, J = 1.9 Hz, 2H), 6.98 (d, J = 1.9 Hz, 2H), 6.97 (d, J = 1.9 Hz, 2H), 6.83 (m, 4H), 6.77 (m, 4H), 6.29 (dd, J = 3.4, 1.2 Hz, 2H), 6.27 (dd, J = 3.4, 1.2 Hz, 2H), 5.27 (s, 1H), 5.20 (d, J = 9.6 Hz, 1H), 4.26 (d, J = 9.6 Hz, 1H), 3.15 (m, 1H), 2.73 (m, 1H), 2.58 (s, 3H), 2.04 (m, 1H), 1.95 (m, 1H), 1.74 (m, 1H), 1.56 (m, 1H), 1.43 (m, 4H), 1.29 (bs, 12H), 0.89 (t, J = 6.8 Hz, 3H). FAB-MS (m/z): $[M]^+$ 1890.4. Elemental analysis calcd (%) for $C_{125}H_{61}N_5S_2Pt{\cdot}H_2O$: C 78.60, H 3.32, N 3.67. Found: C 78.58, H 3.31, N 3.72.

(^{t}Bu-PTZ)$_2$-Pt(bpy)-C$_{60}$. (Yield: 14%). ^{1}H NMR (400 MHz, $CDCl_3$, 50 °C): δ/ppm 9.95 (d, J = 5.7 Hz, 1H), 9.72 (d, J = 5.7 Hz, 1H), 8.59 (bs, 1H), 8.12 (bs, 1H), 8.00 (s, 1H), 7.67 (t, J = 7.7 Hz, 4H), 7.45 (d, J = 5.7 Hz, 1H), 7.22 (d, J = 8.3 Hz, 4H), 7.02 (t, J = 1.8 Hz, 4H), 6.85 (d, J = 8.6 Hz, 4H), 6.23 (dd, J = 8.6, 2.5 Hz, 4H), 5.33 (s, 1H), 5.17 (d, J = 9.7 Hz, 1H), 4.22 (d, J = 9.7 Hz, 1H), 3.13 (m, 1H), 2.73 (m, 1H), 2.56 (s, 3H), 2.03 (m, 1H), 1.93 (m, 1H), 1.72 (m, 1H), 1.48 (m, 5H), 1.29 (bs, 12H), 0.89 (t, J = 6.8 Hz, 3H). FAB-MS (m/z): $[M - 4H]^+$ 2112.1. Elemental analysis calcd (%) for $C_{141}H_{93}N_5S_2Pt{\cdot}2H_2O$: C 78.68, H 4.54, N 3.25. Found: C 78.61, H 4.61, N 3.44.

■ ASSOCIATED CONTENT

Supporting Information

The selected singlet excited states (S_n) computed by TDDFT/CPCM, selected molecular orbitals, transient absorption difference spectra of **di-^{t}BuPhC$_{60}$**, **(PTZ)$_2$-Pt(bpy)** and **(^{t}BuPTZ)$_2$-Pt(bpy)** in CH_2Cl_2, estimation of quantum yields, Cartesian coordinates of the optimized structures, synthesis and characterization of organic ligands and model compounds, and the full form of ref 29. This material is available free of charge via the Internet at http://pubs.acs.org.

■ AUTHOR INFORMATION

Corresponding Authors

wwyam@hku.hk
wm.kwok@polyu.edu.hk

Notes

The authors declare no competing financial interest.

■ ACKNOWLEDGMENTS

V.W.-W.Y. acknowledges support from The University of Hong Kong and the URC Strategic Research Theme on New Materials. This work has been supported by a grant from the Theme-Based Research Scheme (TBRS) of the Research Grants Council of the Hong Kong Special Administrative Region, China (Project No. T23-713/11). We are grateful to the Information Technology Services of The University of Hong Kong for providing computational resources.

■ REFERENCES

(1) (a) Benniston, A. C.; Mackie, P. R.; Harriman, A. *Angew. Chem., Int. Ed. Engl.* **1998**, *37*, 354. (b) Gust, D.; Moore, T. A.; Moore, A. L. *Acc. Chem. Res.* **2000**, *34*, 40. (c) Chakraborty, S.; Wadas, T. J.; Hester, H.; Schmehl, R.; Eisenberg, R. *Inorg. Chem.* **2005**, *44*, 6865. (d) Benniston, A. C. *Phys. Chem. Chem. Phys.* **2007**, *9*, 5739. (e) Fukuzumi, S. *Phys. Chem. Chem. Phys.* **2008**, *10*, 2283. (f) Garg, V.; Kodis, G.; Chachisvilis, M.; Hambourger, M.; Moore, A. L.; Moore, T. A.; Gust, D. *J. Am. Chem. Soc.* **2011**, *133*, 2944. (g) Terazono, Y.; Kodis, G.; Bhushan, K.; Zaks, J.; Madden, C.; Moore, A. L.; Moore, T. A.; Fleming, G. R.; Gust, D. *J. Am. Chem. Soc.* **2011**, *133*, 2916.

(2) (a) Guo, F.; Ogawa, K.; Kim, Y.-G.; Danilov, E. O.; Castellano, F. N.; Reynolds, J. R.; Schanze, K. S. *Phys. Chem. Chem. Phys.* **2007**, *9*, 2724. (b) Flamigni, L.; Collin, J.-P.; Sauvage, J.-P. *Acc. Chem. Res.* **2008**, *41*, 857. (c) Panda, M. K.; Ladomenou, K.; Coutsolelos, A. G. *Coord. Chem. Rev.* **2012**, *256*, 2601.

(3) (a) Flamigni, L.; Barigelletti, F.; Armaroli, N.; Collin, J.-P.; Dixon, I. M.; Sauvage, J.-P.; Williams, J. A. G. *Coord. Chem. Rev.* **1999**, *190–192*, 671. (b) Baranoff, E.; Collin, J.-P.; Flamigni, L.; Sauvage, J.-P. *Chem. Soc. Rev.* **2004**, *33*, 147. (c) Huynh, M. H. V.; Dattelbaum, D. M.; Meyer, T. J. *Coord. Chem. Rev.* **2005**, *249*, 457. (d) Balzani, V.; Bergamini, G.; Marchioni, F.; Ceroni, P. *Coord. Chem. Rev.* **2006**, *250*, 1254. (e) Irebo, T.; Zhang, M.-T.; Markle, T. F.; Scott, A. M.; Hammarström, L. *J. Am. Chem. Soc.* **2012**, *134*, 16247.

(4) (a) Kiyosawa, K.; Shiraishi, N.; Shimada, T.; Masui, D.; Tachibana, H.; Takagi, S.; Ishitani, O.; Tryk, D. A.; Inoue, H. *J. Phys. Chem. C* **2009**, *113*, 11667. (b) Wenger, O. S. *Coord. Chem. Rev.* **2009**, *253*, 1439. (c) Vlček, A., Jr. *Top. Organomet. Chem.* **2010**, *29*, 115. (d) Bingöl, B.; Durrell, A. C.; Keller, G. E.; Palmer, J. H.; Grubbs, R. H.; Gray, H. B. *J. Phys. Chem. B* **2012**, *177*, 4177. (e) Herzog, W.; Bronner, C.; Löffler, S.; He, B.; Kratzert, D.; Stalke, D.; Hauser, A.; Wenger, O. S. *ChemPhysChem* **2013**, *14*, 1168.

(5) (a) Collin, J. P.; Guillerez, S.; Sauvage, J. P.; Barigelletti, F.; De Cola, L.; Flamigni, L.; Balzani, V. *Inorg. Chem.* **1992**, *31*, 4112. (b) De Cola, L.; Belser, P. *Coord. Chem. Rev.* **1998**, *177*, 301. (c) Lainé, P. P.; Campagna, S.; Loiseau, F. *Coord. Chem. Rev.* **2008**, *252*, 2552. (d) Aleman, E. A.; Shreiner, C. D.; Rajesh, C. S.; Smith, T.; Garrison,

S. A.; Modarelli, D. A. *Dalton Trans.* **2009**, 6562. (e) Pichlmaier, M.; Winter, R. F.; Zabel, M.; Záliš, S. *J. Am. Chem. Soc.* **2009**, *131*, 4892. (f) Fortage, J.; Puntoriero, F.; Tuyèras, F.; Dupeyre, G.; Arrigo, A.; Ciofini, I.; Lainé, P. P.; Campagna, S. *Inorg. Chem.* **2012**, *51*, 5342. (g) Hankache, J.; Niemi, M.; Lemmetyinen, H.; Wenger, O. S. *Inorg. Chem.* **2012**, *51*, 6333. (h) Banerjee, T.; Das, A.; Ghosh, H. N. *New J. Chem.* **2013**, *37*, 3100.

(6) (a) Constable, E. C.; Neuburger, M.; Rösel, P.; Schneider, G. E.; Zampese, J. A.; Housecroft, C. E.; Monti, F.; Armaroli, N.; Costa, R. D.; Ortí, E. *Inorg. Chem.* **2012**, *52*, 885. (b) Klein, J. H.; Sunderland, T. L.; Kaufmann, C.; Holzapfel, M.; Schmiedel, A.; Lambert, C. *Phys. Chem. Chem. Phys.* **2013**, *15*, 16024. (c) Wenger, O. S. *Acc. Chem. Res.* **2013**, *46*, 1517.

(7) (a) Ruthkosky, M.; Kelly, C. A.; Zaros, M. C.; Meyer, G. J. *J. Am. Chem. Soc.* **1997**, *119*, 12004. (b) Scaltrito, D. V.; Kelly, C. A.; Ruthkosky, M.; Zaros, M. C.; Meyer, G. J. *Inorg. Chem.* **2000**, *39*, 3765. (c) Li, K.; Bracher, P. J.; Guldi, D. M.; Herranz, M. Á.; Echegoyen, L.; Schuster, D. I. *J. Am. Chem. Soc.* **2004**, *126*, 9156. (d) Ishizuka, T.; Tobita, K.; Yano, Y.; Shiota, Y.; Yoshizawa, K.; Fukuzumi, S.; Kojima, T. *J. Am. Chem. Soc.* **2011**, *133*, 18570. (e) Megiatto, J. D.; Schuster, D. I.; de Miguel, G.; Wolfrum, S.; Guldi, D. M. *Chem. Mater.* **2012**, *24*, 2472.

(8) (a) Chan, C. W.; Lai, T. F.; Che, C. M.; Peng, S. M. *J. Am. Chem. Soc.* **1993**, *115*, 11245. (b) McGarrah, J. E.; Eisenberg, R. *Inorg. Chem.* **2003**, *42*, 4355. (c) Chakraborty, S.; Wadas, T. J.; Hester, H.; Flaschenreim, C.; Schmehl, R.; Eisenberg, R. *Inorg. Chem.* **2005**, *44*, 6284. (d) Suzuki, S.; Sugimura, R.; Kozaki, M.; Keyaki, K.; Nozaki, K.; Ikeda, N.; Akiyama, K.; Okada, K. *J. Am. Chem. Soc.* **2009**, *131*, 10374. (e) Ding, J.; Feng, K.; Tung, C.-H.; Wu, L.-Z. *J. Phys. Chem. C* **2010**, *115*, 833. (f) Lai, S.-W.; Chen, Y.; Kwok, W.-M.; Zhao, X.-J.; To, W.-P.; Fu, W.-F.; Che, C.-M. *Chem.—Asian. J.* **2010**, *5*, 60. (g) Göransson, E.; Boixel, J.; Monnereau, C.; Blart, E.; Pellegrin, Y.; Becker, H.-C.; Hammarström, L.; Odobel, F. *Inorg. Chem.* **2010**, *49*, 9823. (h) Roberts, M. N.; Nagle, J. K.; Majewski, M. B.; Finden, J. G.; Branda, N. R.; Wolf, M. O. *Inorg. Chem.* **2011**, *50*, 4956.

(9) (a) Castellano, F. N.; Pomestchenko, I. E.; Shikhova, E.; Hua, F.; Muro, M. L.; Rajapakse, N. *Coord. Chem. Rev.* **2006**, *250*, 1819. (b) Yoon, S.; Kukura, P.; Stuart, C. M.; Mathies, R. A. *Mol. Phys.* **2006**, *104*, 1275.

(10) (a) Miskowski, V. M.; Houlding, V. H. *Inorg. Chem.* **1989**, *28*, 1529. (b) Lai, S.-W.; Chan, M. C. W.; Cheung, K.-K.; Che, C.-M. *Inorg. Chem.* **1999**, *38*, 4262. (c) Hissler, M.; Connick, W. B.; Geiger, D. K.; McGarrah, J. E.; Lipa, D.; Lachicotte, R. J.; Eisenberg, R. *Inorg. Chem.* **2000**, *39*, 447. (d) McMillin, D. R.; Moore, J. J. *Coord. Chem. Rev.* **2002**, *229*, 113. (e) Yam, V. W.-W.; Wong, K. M.-C.; Zhu, N. *J. Am. Chem. Soc.* **2002**, *124*, 6506. (f) Wong, K. M.-C.; Tang, W.-S.; Chu, B. W.-K.; Zhu, N.; Yam, V. W.-W. *Organometallics* **2004**, *23*, 3459.

(11) (a) Whittle, C. E.; Weinstein, J. A.; George, M. W.; Schanze, K. S. *Inorg. Chem.* **2001**, *40*, 4053. (b) Danilov, E. O.; Pomestchenko, I. E.; Kinayyigit, S.; Gentili, P. L.; Hissler, M.; Ziessel, R.; Castellano, F. N. *J. Phys. Chem. A* **2005**, *109*, 2465. (c) Wong, K. M.-C.; Tang, W.-S.; Lu, X.-X.; Zhu, N.; Yam, V. W.-W. *Inorg. Chem.* **2005**, *44*, 1492. (d) Yam, V. W.-W.; Chan, K. H.-Y.; Wong, K. M.-C.; Zhu, N. *Chem.—Eur. J.* **2005**, *11*, 4535. (e) Wong, K. M.-C.; Yam, V. W.-W. *Coord. Chem. Rev.* **2007**, *251*, 2477. (f) Muro, M. L.; Diring, S.; Wang, X.; Ziessel, R.; Castellano, F. N. *Inorg. Chem.* **2009**, *48*, 11533. (g) Kwok, E. C.-H.; Chan, M.-Y.; Wong, K. M.-C.; Lam, W. H.; Yam, V. W.-W. *Chem.—Eur. J.* **2010**, *16*, 12244.

(12) (a) Maggini, M.; Guldi, D. M.; Mondini, S.; Scorrano, G.; Paolucci, F.; Ceroni, P.; Roffia, S. *Chem.—Eur. J.* **1998**, *4*, 1992. (b) Guldi, D. M.; Maggini, M.; Menna, E.; Scorrano, G.; Ceroni, P.; Marcaccio, M.; Paolucci, F.; Roffia, S. *Chem.—Eur. J.* **2001**, *7*, 1597. (c) Armaroli, N.; Accorsi, G.; Felder, D.; Nierengarten, J.-F. *Chem.—Eur. J.* **2002**, *8*, 2314. (d) Karlsson, S.; Modin, J.; Becker, H.-C.; Hammarström, L.; Grennberg, H. *Inorg. Chem.* **2008**, *47*, 7286. (e) Ventura, B.; Barbieri, A.; Zanelli, A.; Barigelletti, F.; Seneclauze, J. B.; Diring, S.; Ziessel, R. *Inorg. Chem.* **2009**, *48*, 6409.

(13) (a) Martín, N.; Sánchez, L.; Illescas, B.; Pérez, I. *Chem. Rev.* **1998**, *98*, 2527. (b) Guldi, D. M.; Prato, M. *Acc. Chem. Res.* **2000**, *33*, 695. (c) Guldi, D. M. *Chem. Soc. Rev.* **2002**, *31*, 22. (d) Accorsi, G.; Armaroli, N. *J. Phys. Chem. C* **2010**, *114*, 1385.

(14) (a) Chen, P.; Westmoreland, T. D.; Danielson, E.; Schanze, K. S.; Anthon, D.; Neveux, P. E.; Meyer, T. J. *Inorg. Chem.* **1987**, *26*, 1116. (b) Klumpp, T.; Linsenmann, M.; Larson, S. L.; Limoges, B. R.; Bürssner, D.; Krissinel, E. B.; Elliott, C. M.; Steiner, U. E. *J. Am. Chem. Soc.* **1999**, *121*, 1076. (c) Islam, D. M. S.; Sasaki, Y.; Kawauchi, H.; Kozaki, M.; Araki, Y.; Ito, O.; Okada, K. *Bull. Chem. Soc. Jpn.* **2008**, *81*, 103. (d) Sugimura, R.; Suzuki, S.; Kozaki, M.; Keyaki, K.; Nozaki, K.; Matsushita, H.; Ikeda, N.; Okada, K. *Res. Chem. Intermed.* **2012**, *39*, 185.

(15) van Stokkum, I. H. M.; Larsen, D. S.; van Grondelle, R. *Biochim. Biophys. Acta* **2004**, *1657*, 82.

(16) Yonemura, H.; Moribe, S.; Hayashi, K.; Noda, M.; Tokudome, H.; Yamada, S.; Nakamura, H. *Appl. Magn. Reson.* **2003**, *23*, 289.

(17) Suneesh, C. V.; Gopidas, K. R. *J. Phys. Chem. C* **2009**, *113*, 1606.

(18) (a) Skourtis, S. S.; Da Silva, A. J. R.; Bialek, W.; Onuchic, J. N. *J. Phys. Chem.* **1992**, *96*, 8034. (b) Kichigina, A. O.; Ionkin, V. N.; Ivanov, A. I. *J. Phys. Chem. B* **2013**, *117*, 7426.

(19) (a) King, J. C.; Zhang, J. Z.; Schwartz, B. J.; Harris, C. B. *J. Chem. Phys.* **1993**, *99*, 7595. (b) Maçôas, E. M. S.; Kananavicius, R.; Myllyperkiö, P.; Pettersson, M.; Kunttu, H. *J. Phys. Chem. A* **2007**, *111*, 2054.

(20) Al-Subi, A. H.; Niemi, M.; Tkachenko, N. V.; Lemmetyinen, H. *J. Phys. Chem. A* **2012**, *116*, 9653.

(21) Luo, C.; Guldi, D. M.; Imahori, H.; Tamaki, K.; Sakata, Y. *J. Am. Chem. Soc.* **2000**, *122*, 6535.

(22) Marcus, R. A.; Sutin, N. *Biochim. Biophys. Acta* **1985**, *811*, 265.

(23) Meylemans, H. A.; Lei, C.-F.; Damrauer, N. H. *Inorg. Chem.* **2008**, *47*, 4060.

(24) (a) Tkachenko, N. V.; Rantala, L.; Tauber, A. Y.; Helaja, J.; Hynninen, P. H.; Lemmetyinen, H. *J. Am. Chem. Soc.* **1999**, *121*, 9378. (b) Vehmanen, V.; Tkachenko, N. V.; Tauber, A. Y.; Hynninen, P. H.; Lemmetyinen, H. *Chem. Phys. Lett.* **2001**, *345*, 213. (c) Tkachenko, N. V.; Lemmetyinen, H.; Sonoda, J.; Ohkubo, K.; Sato, T.; Imahori, H.; Fukuzumi, S. *J. Phys. Chem. A* **2003**, *107*, 8834.

(25) Kubo, M.; Mori, Y.; Otani, M.; Murakami, M.; Ishibashi, Y.; Yasuda, M.; Hosomizu, K.; Miyasaka, H.; Imahori, H.; Nakashima, S. *J. Phys. Chem. A* **2007**, *111*, 5136.

(26) (a) Closs, G. L.; Miller, J. R. *Science* **1988**, *240*, 440. (b) Newton, M. D. *Chem. Rev.* **1991**, *91*, 767. (c) Newton, M. D.; Sutin, N. *Annu. Rev. Phys. Chem.* **1984**, *35*, 437. (d) Scholes, G. D.; Ghiggino, K. P. *J. Chem. Phys.* **1995**, *103*, 8873. (e) Barbara, P. F.; Meyer, T. J.; Ratner, M. A. *J. Phys. Chem.* **1996**, *100*, 13148. (f) Natali, M.; Campagna, S.; Scandola, F. *Chem. Soc. Rev.* **2014**, *43*, 4005.

(27) (a) Chan, C. T.-L.; Cheng, C. C.-W.; Ho, K. Y.-F.; Kwok, W.-M. *Phys. Chem. Chem. Phys.* **2011**, *13*, 16306. (b) Cheng, C. C.-W.; Ma, C.; Chan, C. T.-L.; Ho, K. Y.-F.; Kwok, W.-M. *Photochem. Photobiol. Sci.* **2013**, *12*, 1351.

(28) Snellenburg, J. J.; Laptenok, S.; Seger, R.; Mullen, K. M.; Stokkum, I. H. M. v. *J. Stat. Software* **2012**, *49*, 1.

(29) Frisch, M. J.; et al. *Gaussian 09*, Revision C.01; Gaussian, Inc.: Wallingford, CT, 2010.

(30) (a) Perdew, J. P.; Burke, K.; Ernzerhof, M. *Phys. Rev. Lett.* **1996**, *77*, 3865. (b) Perdew, J. P.; Burke, K.; Ernzerhof, M. *Phys. Rev. Lett.* **1997**, *78*, 1396. (c) Adamo, C.; Barone, V. *J. Chem. Phys.* **1999**, *110*, 6158.

(31) (a) Stratmann, R. E.; Scuseria, G. E.; Frisch, M. J. *J. Chem. Phys.* **1998**, *109*, 8218. (b) Bauernschmitt, R.; Ahlrichs, R. *Chem. Phys. Lett.* **1996**, *256*, 454. (c) Casida, M. E.; Jamorski, C.; Casida, K. C.; Salahub, D. R. *J. Chem. Phys.* **1998**, *108*, 4439.

(32) (a) Barone, V.; Cossi, M. *J. Phys. Chem. A* **1998**, *102*, 1995. (b) Cossi, M.; Rega, N.; Scalmani, G.; Barone, V. *J. Comput. Chem.* **2003**, *24*, 669.

(33) Andrae, D.; Häußermann, U.; Dolg, M.; Stoll, H.; Preuß, H. *Theor. Chim. Acta* **1990**, *77*, 123.

(34) Ehlers, A. W.; Böhme, M.; Dapprich, S.; Gobbi, A.; Höllwarth, A.; Jonas, V.; Köhler, K. F.; Stegmann, R.; Veldkamp, A.; Frenking, G. *Chem. Phys. Lett.* **1993**, *208*, 111.
(35) (a) Hehre, W. J.; Ditchfield, R.; Pople, J. A. *J. Chem. Phys.* **1972**, *56*, 2257. (b) Hariharan, P. C.; Pople, J. A. *Theor. Chim. Acta* **1973**, *28*, 213. (c) Francl, M. M.; Pietro, W. J.; Hehre, W. J.; Binkley, J. S.; Gordon, M. S.; DeFrees, D. J.; Pople, J. A. *J. Chem. Phys.* **1982**, *77*, 3654.
(36) Aldridge, W. S.; Hornstein, B. J.; Serron, S.; Dattelbaum, D. M.; Schoonover, J. R.; Meyer, T. J. *J. Org. Chem.* **2006**, *71*, 5186.
(37) Wessendorf, F.; Grimm, B.; Guldi, D. M.; Hirsch, A. *J. Am. Chem. Soc.* **2010**, *132*, 10786.
(38) Greci, L.; Mar'in, A.; Stipa, P.; Carloni, P. *Polym. Degrad. Stab.* **1995**, *50*, 305.